Laser guide star multi-conjugate adaptive optics performance of the Thirty Meter Telescope with elongated beacons and matched filtering

Luc Gilles, Brent Ellerbroek, Jean-Pierre Véran

Luc Gilles, Brent Ellerbroek, Jean-Pierre Véran, "Laser guide star multi-conjugate adaptive optics performance of the Thirty Meter Telescope with elongated beacons and matched filtering," Proc. SPIE 6272, Advances in Adaptive Optics II, 627236 (28 June 2006); doi: 10.1117/12.671511

SPIE.

Event: SPIE Astronomical Telescopes + Instrumentation, 2006, Orlando, Florida , United States

Laser guide star multi-conjugate adaptive optics performance of the Thirty Meter Telescope with elongated beacons and matched filtering

Luc Gilles[a], Brent Ellerbroek[a] and Jean-Pierre Véran[b]

[a]Thirty Meter Telescope Project Office
1200 E. California Boulevard, Mail Code 102-8
Pasadena, CA 91125
[b]Herzberg Institute of Astrophysics,
5071 West Saanich Road, Victoria, British Columbia, Canada

ABSTRACT

This paper describes wave-optics Monte Carlo simulation results to asses the impact of laser guide star wavefront sensor nonlinearity with elongated sodium beacons on the residual wavefront error for the Thirty Meter Telescope Narrow Field InfraRed Adaptive Optics System, which is a laser guide star multi-conjugate adaptive optics system intended to provide near-diffraction limited performance in the near infrared over a 30 arcsec diameter field of view.

Keywords: Sodium laser guide star elongation, Shack-Hartmann wavefront sensor nonlinearity

1. INTRODUCTION

The Thirty Meter Telescope (TMT) is currently in its conceptual design phase [1]. TMT will strongly depend on its Narrow Field InfraRed Adaptive Optics System (NFIRAOS) [2,3] to reach its maximal sky coverage and full diffraction limited capability in the near infrared. The baseline design envisions NFIRAOS as a 6 sodium laser guide star system [4] of order 60 sensing and correction. A powerful real-time controller [5] will process a total of 120,000 active CCD pixels per LGS WFS and compute 7,500 deformable mirror (DM) commands distributed between a DM conjugate to ground level and another conjugate to a 12 km altitude in the atmosphere at a rate of up to 800 Hz.

LGS AO on a 30 m aperture raises several challenging technical issues related to the finite range of the beacon and its three dimensional structure. Light rays from a finite range LGS probe a cone of atmosphere, not a cylindar like from a natural guide star (NGS), an effect known as focal anisoplanatism [6]. Multiple LGS's (laser tomography adaptive optics) can remove this effect but add complexity to the system. Sodium LGS's use the mesospheric sodium layer as back-scatter. This layer is located at a mean altitude of $h_{\rm Na} = 90$ km and has a mean thickness of $\sigma_{\rm Na} = 10$ km. As a result, a sodium LGS will have vertical extension, i.e. perspective elongation, and a Shack-Hartmann wavefront sensor (SH-WFS) subaperture image of such a laser beacon will be elongated. The angular subtense of the beacon along the elongation direction, θ_{Na}, increases approximately proportionally to the distance between the subaperture and the laser launch telescope (LLT), the thickness of the layer, and decreases proportionally to the inverse of the square of the profile mean altitude: $\theta_{Na} \approx r_{\rm SA}\,\sigma_{\rm Na}/h_{\rm Na}^2$. For TMT, the LLT will be located behind the secondary mirror, producing radially elongated LGS subaperture focal plane spots. $h_{\rm Na}$, $\sigma_{\rm Na}$ and the detailed structure of the sodium profile all evolve significantly on time scales of seconds to minutes. For edge subapertures of the TMT ($r_{\rm SA} = 14.5$ m), the average angular size of the beacon along the radial direction is on the order of $\theta_{Na} \sim 3$ arcsec, which is at least 3 times larger than the seeing-limited angular size of the spots observed with NGS's. Further complications introduced by the finite range and vertical extension of sodium LGS's are: (i) sodium layer altitude variations tracking [7] and (ii) focus range mismatch between the telescope focus at infinity and the extended finite range LGS's.

Send correspondence to lgilles@caltech.edu

Advances in Adaptive Optics II, edited by Brent L. Ellerbroek, Domenico Bonaccini Calia,
Proc. of SPIE Vol. 6272, 627236, (2006) · 0277-786X/06/$15 · doi: 10.1117/12.671511

This paper presents sample Monte Carlo wave-optics simulation results to assess the impact of LGS WFS spot position estimation algorithm nonlinearity on NFIRAOS residual wavefront error. Two subaperture spot position estimation algorithms are considered: the standard centroiding algorithm and a noise-optimal matched filter [8]. Simulations were performed in LAOS, a Matlab end-to-end Linear Adaptive Optics Simulator using sparse matrix techniques to compute efficiently a minimum variance wavefront reconstructor [9]. Curiously, we find that matched filtering introduces spikes in the residual wavefront error time history when perspective elongation is present, a behaviour that is presently not well understood and requires further investigation. Assuming infinite linear dynamic range LGS WFS's, the residual wavefront error accounting for the combined effects of WFS sampling, tomography, DM fitting and servo lag errors is found on the order of 118 nm on-axis and 124 nm when averaged over a 10 arcsec x 10 arcsec FoV and 1200 frames of data (1.5 sec). The additional root sum square (RSS) wavefront error due to LGS WFS nonlinearity for the centroid/matched filter algorithms is found on the order of 28 nm/58 nm on-axis and 29 nm/61 nm when averaged over the FoV.

The paper is organized as follows: section 2 provides an overview of LAOS, sample simulation results are presented in section 3, and section 4 concludes the study.

2. LAOS OVERVIEW AND LGS WAVE-OPTICS CAPABILITIES

The original features of LAOS are summarized in Table 1, which also outlines current capabilities and planned upgrades to support more detailed modeling of LGS AO systems. The current LGS WFS modeling capabilities in column 3 were used to generate the results presented in this paper. In its original implementation developed by Ellerbroek [10], all AO components and phenomena were based upon linear (i.e. first-order) models and were anchored against analytical first-order performance estimates for 8 m class telescopes. In its current implementation, LAOS is able to perform detailed wave-optics simulations of single conjugate AO (SCAO, i.e. one LGS and one DM), multi conjugate AO (MCAO, i.e. several LGS's and several DM's), laser tomography AO (LTAO, i.e. several LGS's but only one DM), multi object AO (MOAO, i.e. several LGS's and one DM per field point), and ground layer AO (GLAO, i.e. improved seeing when turbulence is concentrated near the ground). The modular structure of LAOS is illustrated in Fig.1. The LGS pointing loop and wave-optics WFS modules were developed to assess the impact of LGS WFS nonlinearity as well as of higher-order speckle noise effects. The AO loop can be closed on either the geometric or wave-optics gradients at any simultaion time step. In the later case, the user can select as subaperture tilt reconstructor either a conventional centroid algorithm with gain optimization or a pre-computed matched filter. Both reconstructors together with the LGS WFS model are detailed in Ref.8.

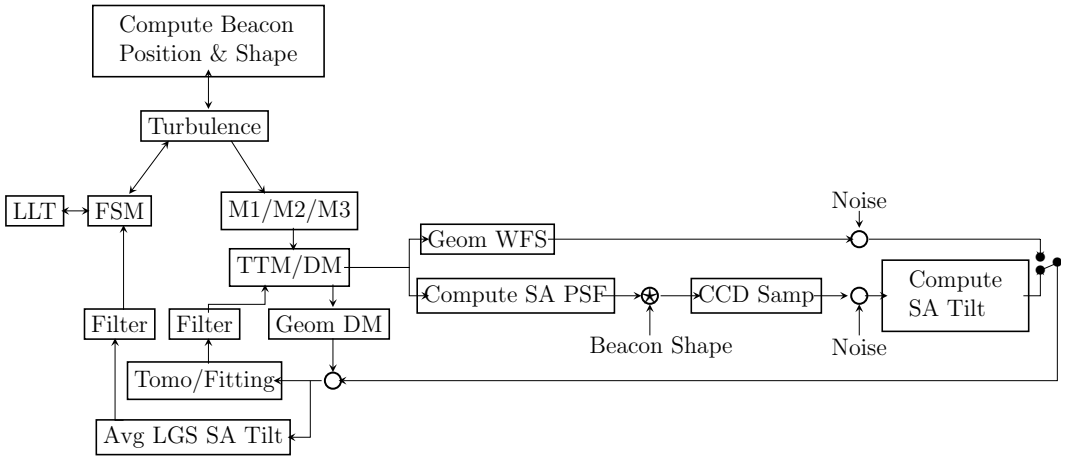

Figure 1. Illustration of the modular structure of LAOS.

Table 1. Existing and planned LAOS modeling capabilities

	Initial Implementation	Current Capabilities	Planned Upgrades
AO Modes	• SCAO, LTAO, MCAO	• GLAO, MOAO	
Trade space limits	• Order 60×60 MCAO	• Order 120×120 MCAO and MOAO	
wavefront disturbances	• Von Karman atmospheric phase screens • Taylor frozen flow temporal dynamics	• Static telescope aberrations • Non-common path aberrations	• Low-order dynamic telescope aberrations
Telescope pupil	• Circular with circular obscuration		• Arbitrary amplitude profile (non-circular)
Reconstruction algorithms	• Pseudo open loop, minimum variance tomographic wavefront estimation (computationally efficient multi-grid implementation) • RMS best fit of actuator influence functions to the estimated turbulence profile		• Fourier domain reconstructor
Control system architectures	• Common temporal filter for all DM's and actuators	• Tip/tilt mirror loop and tip/tilt tweeter loop	• Woofer-tweeter higher order control
WFS modeling	• Subaperture averaged wavefront gradients plus additive gaussian noise	• Wave-optics NGS SH-WFS's • Wave-optics LGS SH-WFS's with uplink propagation, laser pointing loop and beacon elongation • Photon statistics and detector read-out noise • Centroiding • Matched filtering • Radial format CCD	• Anisoplanatic beacon modeling • Pupil misregistration • Correlation tracking
DM Modeling	• Linear superposision of bilinear influence functions	• Hysteresis • Finite stroke	• Pupil misregistration • Modal low-order influence functions for bimorph mirrors and adaptive secondary mirrors
Performance	• RMS wavefront	• Time averaged PSF's	

3. DISCUSSION

We report in this section sample LAOS wave-optics simulation results assessing the impact of LGS WFS nonlinearity on residual wavefront error for NFIRAOS. The main features of the simations are:

- 1 geometrical-optics tip/tilt/focus/astigmatism NGS SH-WFS (order 2×2) to sense low-order modes.
- 6 wave-optics LGS SH-WFS's (order 60×60) to sense higher-order modes.

- 0.5 m diameter LLT located behind the secondary mirror, projecting 6 gaussian laser beams of $1/e^2$ intensity diameter equal to 0.3 m.
- 6 atmospheric optical path differences (OPD's) with von Karman statistics on grids of resolution equal to 1/32 m with Taylor frozen flow temporal dynamics scaled to provide a Fried parameter equal to $r_0(\lambda_0 = 500\,\text{nm}) = 0.15$ m, and an isoplanatic angle equal to $\theta_0(\lambda_0 = 500\,\text{nm}) = 2.65$ arcsec. Turbulence outer-scale equal to $L_0 = 30$ m.
- Geometric ray propagation through atmospheric OPD's, TTM and DM's to aperture-plane grid of 1/32 m resolution.
- 800 Hz sampling, identical double-pole type 1 servos for the DM, TTM and fast steering mirror (FSM) loops with gain of 0.5 and 1 frame (1.25 ms) latency.
- Radial format CCD array (subaperture focal plane pixels aligned alond the elongation direction) with 16×4 500 mas pixels per subaperture for each LGS WFS [11].
- LGS WFS subaperture spots computed from far field Fraunhofer propagator applied to subaperture field sampled at resolution of 1/64 m on a 1 m x 1 m grid providing Nyquist sampling and 7.8 arcsec bandwidth at 589 nm.
- Matched filter and centroid spot position estimation algorithms precomputed from short-exposure theory (perfectly tip/tilt compensated subaperture Kolmogorov OPD's) for the two sodium profiles displayed in Fig.2, a signal level of 1000 photo-detected electrons per frame, and no read noise (see Ref.8 for details).
- No photon nor read noise in the CCD pixel intensities in the wave-optics simulations in order to isolate the effects of LGS WFS nonlinearity.
- Noise-free geometric gradients (infinite SNR).
- Common tomographic wavefront reconstructor incorporating uniform 15 mas regularization noise for the LGS WFS's and $20\,(0.5/15)\,\sqrt{4/\pi} = 0.75$ mas regularization noise for the tip/tilt/focus WFS.
- Identical static sodium profile used to precompute the subaperture tilt reconstructors and to simulate the subaperture spots.
- Laser focused at sodium profile centroid.

Figure 2 displays the average sodium profile (FWHM on the order of 10 km) obtained by shifting and averaging 88 LIDAR sodium profile measurements with temporal and spatial resolution equal to 72 sec and 24 m respectively [12], superimposed on top of a narrow theoretical gaussian profile (FWHM equal to 0.16 km).

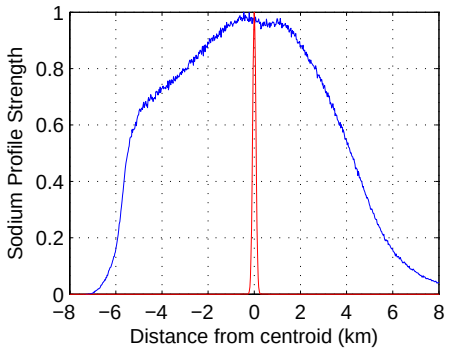

Figure 2. Average sodium profile (FWHM on the order of 10 km) obtained by shifting and averaging 88 LIDAR sodium profile measurements with temporal and spatial resolution equal to 72 sec and 24 m respectively [12], superimposed on top of a narrow theoretical gaussian profile (FWHM equal to 0.16 km).

Figure 3 dipslays colormaps of the centroid and short-exposure matched filter subaperture tilt estimators for a central (top row) and an edge subaperture (bottom row) of the TMT. The most salient feature of the matched filter pixel weights is their concentration at pixels where the derivative of the short-exposure reference nominal image (last column) is large.

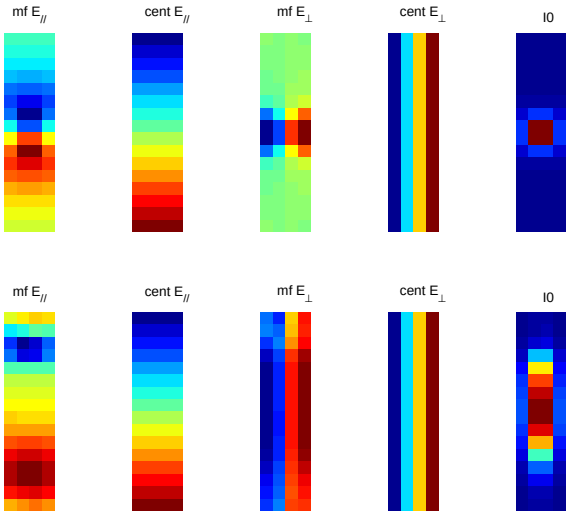

Figure 3. Illustration of subaperture centroid and matched filter tilt estimators. See Ref.8 for details. The ||- and ⊥ subscripts refer to the radial and azimuthal directions.

Fig.4 displays time histories of tilt-included and tilt-removed residual wavefront errors averaged over a 10 arcsec x 10 arcsec FoV, accounting for WFS sampling, tomography, DM fitting, servo lag and LGS WFS nonlinearity wavefront errors.

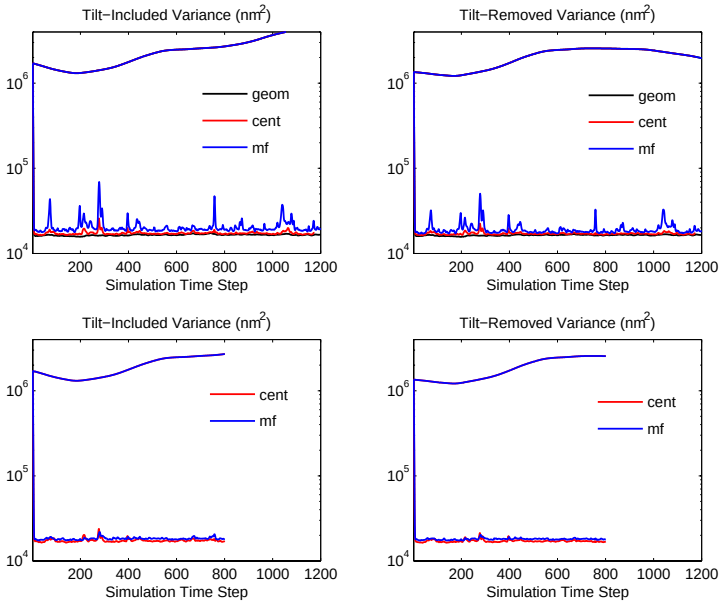

Figure 4. Top panels: Tilt-included and tilt-removed residual wavefront error time history averaged over the NFIRAOS 10 arcsec x 10 arcsec FoV for the 10 km thick sodium profile displayed in Fig.2. Bottom panels: same as top panels but for the theoretical 0.16 km thick gaussian sodium profile displayed in Fig.2.

Averaged over 1200 frames of data (1.5 sec), the RMS tilt-included error for the geometric simulation (infinite WFS linear dynamic range) is found equal to 118 nm on-axis and 124 nm over a 10 arcsec x 10 arcsec FoV The additional root sum square (RSS) wavefront error due to LGS WFS nonlinearity for the centroid/matched filter algorithms is found on the order of 28 nm/58 nm on-axis and 29 nm/61 nm over the FoV. Curiously, the matched filter algorithm gives rise to spikes in the residual wavefront error time history when perspective elongation is present. The reasons for this behaviour are presently not well understood. The fact that these spikes are not seen when perspective elongation is not present (which is almost the case for the 0.16 km thick sodium profile), seems to indicate that the lack of linear dynamic range of the matched filter [8] may perhaps not be the only explanation. In order to gain insight into this problem, Fig.5 displays a frame near the peak of the first spike in Fig.4 of geometric gradients and matched filter errors for the WFS that had the most severe errors.

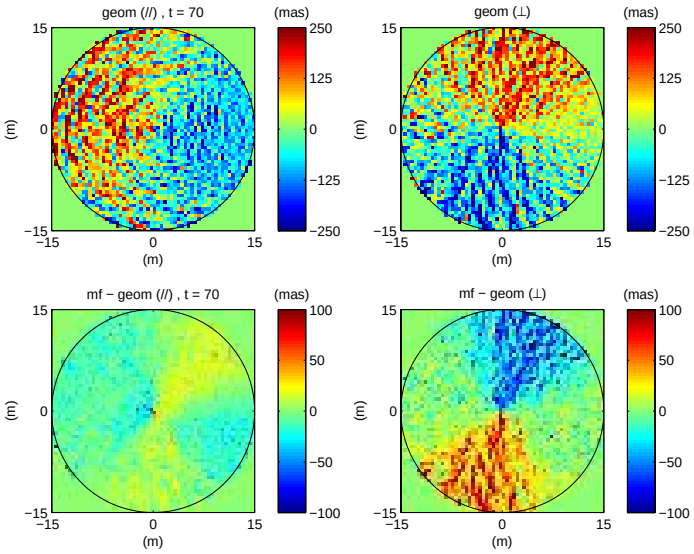

Figure 5. Sample frame near the first spike in Fig.4 of geometric gradients and matched filter errors.

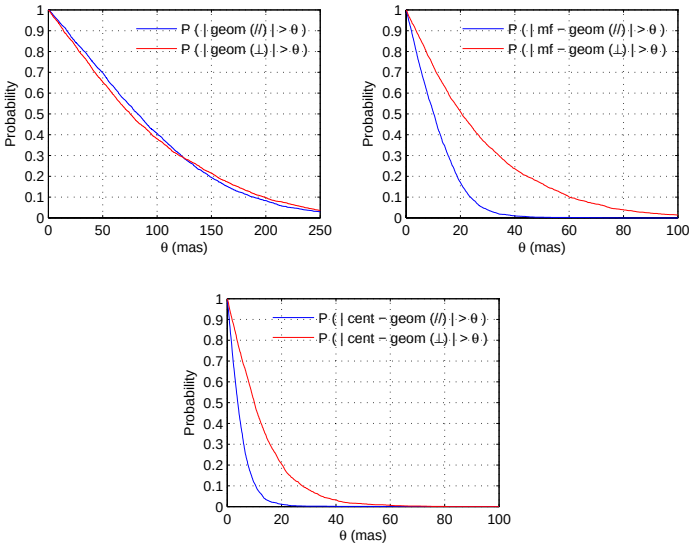

Figure 6. Sample complement of cumulative probability distribution of geometric gradients, matched filter and centroid errors for the same frame of LGS WFS pixels used in Fig.5.

It is seen that subaperture tilts in the azimuthal ($\perp$) direction are underestimated. We have verified that a CCD array with 16 x 6 500 mas pixels per subaperture does not help improve the problem. Finally, Fig.6 displays the complement of the cumulative probability distribution of geometric gradients, matched filter and centroid errors for the same frame of LGS WFS pixels used in Fig.5. It is seen than 90% of the subapertures have tilts smaller than 200 mas, but yet 50% of them have matched filter errors greater than 20 mas in the $\perp$-direction.

4. CONCLUSIONS

Sodium LGS SH-WFS spot elongation is a significant challenge for future extremely large telescopes such as the TMT. This paper presented sample wave-optics Monte Carlo residual wavefront error time histories for NFIRAOS using LAOS, a powerful Matlab end-to-end Linear Adaptive Optics Simulator, to assess the impact of LGS SH-WFS spot position estimation nonlinearity. The wavefront errors due to centroid/mathced filter nonlinearity were found equal to 28 nm/58 nm on-axis and 29 nm/61 nm over a 10 arcsec x 10 arcsec FoV. Further analysis is required to understand the poor behaviour of mached filtering in the presence of perspective elongation.

Acknowledgments

Authors acknowledge the Purple Crow Lidar team from the University of Western Ontaria, Canada, for making their sodium layer measurements available to us. The authors gratefully acknowledge the support of the TMT partner institutions. They are the Association of Canadian Universities for Research in Astronomy (ACURA), the Association of Universities for Research in Astronomy (AURA), the California Institute of Technology and the University of California. This work was supported, as well, by the Canada Foundation for Innovation, the Gordon and Betty Moore Foundation, the National Optical Astronomy Observatory, which is operated by AURA under cooperative agreement with the National Science Foundation, the Ontario Ministry of Research and Innovation, and the National Research Council of Canada.

REFERENCES

1. J.E.Nelson and G.H.Sanders, "TMT status report," in Ground-based and Airborne Telescopes, L. M. Stepp, ed., Proc. SPIE **6267,** (2006).
2. G.Herriot, "NFIRAOS: TMT narrow-field near-infrared facility adaptive optics," in Advances in Adaptive Optics II, B.L.Ellerbroek and D.B.Calia, eds., Proc. SPIE **6269,** (2006).
3. B.L.Ellerbroek et al. "A conceptual design for the Thirty Meter Telescope adaptive optics systems," in Advances in Adaptive Optics II, B.L.Ellerbroek and D.B.Calia, eds., Proc. SPIE **6269,** (2006).
4. R.R.Joyce, C.Boyer, L.G.Daggert, B.L.Ellerbroek, A.Hileman, M.R.Hunten and M. Liang, "The laser guide star facility for the Thirty Meter Telescope," in Advances in Adaptive Optics II, B.L.Ellerbroek and D.B.Calia, eds., Proc. SPIE **6269,** (2006).
5. C.Boyer, B.L.Ellerbroek, G.Herriot, S.L.Browne, and G.A.Tyler, "TMT adaptive optics systems control architecture," in Advances in Adaptive Optics II, B.L.Ellerbroek and D.B.Calia, eds., Proc. SPIE **6269,** (2006).
6. D.L.Fried and J.F.Belsher, "Analysis of fundamental limits to artificial-guide-star adaptive optics system performance for astronomical imaging," J. Opt. soc. Am. A **11**, 277-287 (1994).
7. G.Herriot, P.Hickson, B.L.Ellerbroek, and C.Y.She, "Focus errors from tracking sodium layer altitude variations with laser guide star adaptive optics for the Thirty Meter Telescope," in Advances in Adaptive Optics II, B.L.Ellerbroek and D.B.Calia, eds., Proc. SPIE **6269,** (2006).
8. L.Gilles and B.L.Ellerbroek, "Laser guide star Shack-Hartman wavefront sensor modeling: matched filtering, wavefront sensor nonlinearity, and impact of sodium layer variability for the Thirty Meter Telescope," in Advances in Adaptive Optics II, B.L.Ellerbroek and D.B.Calia, eds., Proc. SPIE **6269,** (2006).
9. L.Gilles and B.L.Ellerbroek, "LAOS: Linear Adaptive Optics Simulator," available from authors upon request.
10. B.L.Ellerbroek, L.Gilles, and C.R.Vogel, "Numerical Simulations of Multiconjugate Adaptive Optics Wavefront Reconstruction on Giant Telescopes," Appl. Opt. **42,** 4811-4818 (2003).

11. J.W.Beletic, "Follow the Yellow-Orange Rabbit: A CCD optimized for wavefront sensing a pulsed sodium laser guide star," Proc. SPIE **5499,** 302–309 (2004).
12. P.S.Argall, R.J.Sica, O.Vassiliev and M.M.Mwangi, "Lidar measurements taken with a large-aperture liquid mirror: Sodium resonance-fluorescence system," Appl. Opt. **39,** 2393–2399 (2000).